LBL-36558
UC-401

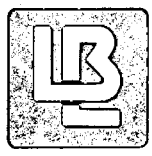

Lawrence Berkeley Laboratory
UNIVERSITY OF CALIFORNIA

CHEMICAL SCIENCES DIVISION

To be published as a chapter in *Atomic, Molecular and Optical Physics Reference Book*, G. Drake, Ed., American Institute of Physics, New York, NY, 1994

Reactive Scattering

A.G. Suits and Y.T. Lee

December 1994

Prepared for the U.S. Department of Energy under Contract Number DE-AC03-76SF00098

DISCLAIMER

LBL-36558
UC-401

Reactive Scattering

Arthur G. Suits and Yuan T. Lee

Chemical Sciences Division
Lawrence Berkeley Laboratory
University of California
Berkeley, California 94720

December 1994

This work was supported by the Director, Office of Energy Research, Office of Basic Energy Sciences, of the U.S. Department of Energy under Contract No. DE-AC03-76SF00098.

56

Reactive Scattering

Arthur G. Suits and Yuan T. Lee

Lawrence Berkeley Laboratory

56.1	**INTRODUCTION**		**1**
56.2	**EXPERIMENTAL METHODS**		**1**
	56.2.1	Molecular Beam Sources	1
	56.2.2	Reagent Preparation	2
	56.2.3	Detection of Neutral Products	3
	56.2.4	A Typical Signal Calculation	5
56.3	**EXPERIMENTAL CONFIGURATIONS**		**5**
	56.3.1	Crossed-beam Rotatable Detector	5
	56.3.2	Doppler Techniques	6
	56.3.3	Product Imaging	7
	56.3.4	Laboratory to Center-of-Mass Transformation	8
56.4	**ELASTIC AND INELASTIC SCATTERING**		**10**
	56.4.1	Introduction	10
	56.4.2	The Differential Cross Section	10
	56.4.3	Rotationally Inelastic Scattering	10
	56.4.4	Vibrationally Inelastic Scattering	11
	56.4.5	Electronically Inelastic Scattering	11
56.5	**REACTIVE SCATTERING**		**11**
	56.5.1	Introduction	11
	56.5.2	Harpoon/stripping reactions	11
	56.5.3	Rebound reactions	12
	56.5.4	Long-lived complexes	12

56.1 INTRODUCTION

This chapter presents a resume of the methods commonly employed in scattering experiments involving neutral molecules at chemical energies, i.e., less than about 10 eV. These experiments include the study of intermolecular potentials, the transfer of energy in molecular collisions and elementary chemical reaction dynamics. Closely related material is presented in Chapters 27, 28, and 33 as well as in other chapters in sections V and VI.

56.2 EXPERIMENTAL METHODS

56.2.1 Molecular Beam Sources

The development of molecular beam methods in the past two decades has transformed the study of chemical physics[1]. Supersonic molecular beam sources allow one to prepare reagents possessing a very narrow velocity distribution with very low internal energies, ideal for use in detailed studies of intermolecular interactions. Early experiments generally employed continuous beam sources but in recent years intense pulsed beam sources

have come into common use[2]. The advantages of pulsed beams primarily arise from the lower gas loads associated with their use, hence reduced demands on the pumping system. If any component of the experiment is pulsed (pulsed laser detection, for example) then considerable advantage may be obtained by employing pulsed beams over continuous beams. Although the theoretical descriptions of pulsed and continuous expansions are essentially equivalent, in practice some care is required in employing pulsed beams because the temperature and velocity distributions may change dramatically through the course of the pulse. Free jet expansions are "supersonic" because the dramatic drop in the local temperature in the beam is associated with a drop in the local speed of sound. A detailed description of the supersonic expansion may be found in references [3, 4, 5]. In practice, many of the detailed features associated with a supersonic expansion may be ignored and one may assume an isentropic expansion into the vacuum. For an isentropic nozzle expansion of an ideal gas the maximum terminal velocity is given by

$$V_{max} = \sqrt{\frac{2k}{m}(\frac{\gamma}{\gamma-1})T_o} \tag{56.1}$$

or

$$V_{max} = \sqrt{\frac{2\hat{C}_p T_o}{m}} \tag{56.2}$$

where for an ideal gas the heat capacity is

$$\hat{C}_p = (\frac{\gamma}{\gamma-1})\frac{k}{m}, \tag{56.3}$$

k is Boltzmann's constant, m is the molecular mass,T_o the temperature in the stagnation region and γ the heat capacity ratio. For ideal gas mixtures assuming C_p independent of temperature for the range encountered in the expansion one may use

$$\bar{C}_p = \sum_i X_i C_{p_i} = \sum_i X_i(\frac{\gamma_i}{\gamma_i-1})R \tag{56.4}$$

and the average molar mass

$$\bar{m} = \sum_i X_i m_i \tag{56.5}$$

where X_i is the mole fraction of component i, to obtain an estimate of the maximum velocity for a mixture:

$$V_{max} = \sqrt{\frac{2\bar{C}_p T_o}{\bar{m}}}. \tag{56.6}$$

By seeding heavy species in light gases one may accelerate them to superthermal energies. Supersonic beams are characterized by the speed ratio, i.e., the mean velocity divided by the velocity spread:

$$S \equiv \frac{V}{\sqrt{\frac{kT}{m}}} \tag{56.7}$$

where T is the local translational temperature, or by the Mach number:

$$M \equiv \frac{V}{\sqrt{\frac{\gamma kT}{m}}}. \tag{56.8}$$

For the purpose of order-of-magnitude calculations, the number density on axis far from the nozzle may be estimated as

$$n \approx n_o(\frac{d}{x})^2 \tag{56.9}$$

where n_o is the number density in the stagnation region, d is the nozzle diameter and x is the distance from the nozzle. The number density-speed distribution of a nozzle beam is well described as a Gaussian characterized by the speedratio S and a parameter $\alpha = V_o/S$, where V_o is the most probable velocity:

$$n(v) = v^2 e^{-(\frac{v}{\alpha}-S)^2}. \tag{56.10}$$

Cooling efficiencies for the various internal degrees of freedom correlate with the efficiency of coupling of these modes with translation, hence they vary widely. Coupling of modes A and B is expressed by the "collision number" Z_{A-B}:

$$Z_{A-B} \equiv Z\tau_{A-B} \tag{56.11}$$

where τ_{A-B} is the bulk relaxation time and Z the collision frequency. This represents the number of collisions between effective inelastic events. Typical values are summarized in Table 56.1. R-T coupling is relatively efficient, while V-T coupling is quite inefficient, so that vibrational excitation may not be effectively cooled in the expansion.

56.2.2 Reagent Preparation

Molecular beam methods may be used in conjunction with a variety of other techniques to prepare atoms or molecules in excited or polarized initial states ??, to generate unstable molecules or radicals[6, 7] or to produce beams of refractory materials such as transition metals or carbon[8, 9]. Some of the common techniques are outlined below. Optical pumping of atoms to excited electronic states is a useful means of reagent preparation,

Table 56.1. Collision numbers for coupling between different modes. V, R, T refer to vibrational, rotational and translational energy, respectively. Entry is the typical range of Z_{A-B}.

	V	R	T
V	10^{5-3}	10^{3-4}	10^{5-6}
R		10^{0-1}	10^{2-3}

and this topic is presented in detail in Chapter ??. This technique further allows one, using polarized lasers, to explore the influence of angular momentum polarization in the reagents on the collision dynamics. Most of these studies have been performed using alkali and alkaline earth metals since there exist strong electronic transitions and convenient narrow-band visible lasers suitable for use with these systems. Laser excitation may also be used to generate vibrationally excited molecules in their ground electronic states. The techniques employed include direct IR excitation using an HF chemical laser[10], population depletion methods[11] and various Raman techniques[12].

Metastable atoms may also be prepared by laser photolysis of a suitable precursor. $O(^1D)$ is readily prepared by photolysis of ozone or N_2O, for example[49]. Alternatively, radio frequency or microwave discharge may be used to produce metastable species or reactive atoms or radicals[13]. These techniques may also be used to prepare ground state atoms; for example hot H atom beams are frequently produced by photolysis of HI or H_2S [14]. Such atomic or molecular radical beams may also be generated by pyrolysis in the nozzle. In this case care must be taken to minimize recombination through careful choice of the temperature, nozzle geometry and transit time through the heated region.

Beams of refractory materials are now commonly generated using laser ablation sources[8, 9]. Typically these employ a rod or disk of the substrate of interest which is simultaneously rotated and translated to provide a fresh surface for ablation at each laser pulse. A laser beam is focused on the substrate and timed to fire just as a carrier gas pulse passes over. Laser power and wavelength must be optimized for a given substrate. Lasers operating in the infrared, visible and ultraviolet have all been employed.

Aligned or oriented molecules have been prepared using multipole focussing[15, 16] and more recently using strong electric fields ("brute force"). [17] In the former case, specific quantum states are focused by the field. In the latter case so-called pendular states are prepared from the low rotational levels of molecules possessing large dipole moments and small rotational constants. The ability to orient these molecules can be estimated on the basis of the Stark parameter $\omega = \mu E/B$, where μ is the dipole moment, E the electric field strength, and B the rotational constant. Orientation is feasible for low rotational levels of molecules when the Stark parameter is on the order of 10 or higher[17].

56.2.3 Detection of Neutral Products

Broadly speaking, detection of neutral molecules is accomplished either by optical (spectroscopic) or nonoptical techniques. Nonoptical methods usually involve non-specific ionization of neutral particles, most commonly by electron impact, followed by mass selection and ion counting. Thermal detectors such as cryogenic bolometers are also finding widespread application in molecular beam experiments owing to their remarkable sensitivity[18]. In general, optical methods may rely on resonant or non-resonant processes, hence they may or may not enjoy quantum state selectivity. Both photoionization and laser-induced fluorescence methods are now in common use, usually in applications where quantum state resolved information is desired. The advantage of nonoptical methods is primarily one of generality: all neutral molecules may be detected and branching into different channels readily measured. Quantum state resolution is more difficult to achieve using nonoptical detection methods, but both vibrationally- and rotationally-resolved measurements have been obtained by these means[19, 44].

The primary advantage of spectroscopic detection is the aforementioned possibility of quantum state specificity. Another unique experimental opportunity afforded by spectroscopic probes is the measurement of product aligment and orientation. In addition in some cases background interference may be reduced or eliminated using state-specific probes, thereby affording enhanced signal-to- noise ratios.

Nonoptical Techniques

Detectors based on nonspecific ionization remain the most common employed in molecular beam experiments owing to the ease of subsequent mass selection and the convenience and sensitivity of ion detection. Surface ionization is a sensitive means of detecting alkali atoms and other species exhibiting low ionization potentials[21]. The sensitivity of the technique led to its widespread use in the early days of crossed-beam experiments, and it is the reason that the dynamics of alkali atom collisions were studied in such depth. Surface ionization occurs when a neutral atom or molecule with a low ionization potential sticks on a surface with a high work function and is subsequently desorbed. Typically these detectors employ a hot platinum or oxidized tungsten wire or ribbon for formation and subsequent desorption of the ions, which is surrounded by an ion collector. They are very efficient for the detection of alkali atoms and molecules whose ionization potentials are below about 6 eV.

All neutral gas molecules may be ionized by collision with energetic electrons, and electron beam ionizers may be produced that couple conveniently to quadrupole mass spectrometers[38]. Collision of a molecule with a 100-200 eV electron leads predominantly to formation of the positive ion and a secondary electron. Other processes also occur and can be very significant: doubly or triply charged ions may be formed and, importantly, molecules

can fragment yielding many daughter ions in addition to the parent ion. These fragmentation patterns vary with different molecules, and may further show a strong dependence on molecular internal energy, so particular care must be taken to determine the role of these phenomena in each particular experimental application. It is often necessary to record data for the parent ion and daughter ions for a given product channel and compare them to eliminate contributions arising from cracking of the parent molecule or other species.[23] Electron impact ionization probabilities for most species exhibit a similar dependence on electron energy, rising rapidly from the ionization potential to a peak at 80-100 eV, then falling more slowly with subsequent increase in collision energy. The ionization probability for different species scales with molecular polarizability according to a well-established empirical relation[24]:

$$\sigma_{ion} = 36\sqrt{\alpha} - 18 \qquad (56.12)$$

where σ_{ion} is in square angstroms and α, the molecular polarizability, is in cubic angstroms. This relation can be used to estimate branching ratios in the absence of any other means of calibrating the relative contributions of two different channels. The ionization rate is given by

$$\frac{d[M^+]}{dt} = I_e \sigma [M] \qquad (56.13)$$

where I_e is the electron beam intensity, typically 10 mA/cm^2 or 6×10^{16} electrons/cm^{2}s, and $[M]$ is the number density of molecules M in the ionizer. If one assumes an ionization cross section σ_{ion} of 10^{-16} cm^2 for collision with 150 eV electrons (a typical value for a small molecule), the ionization probability for molecules residing in the ionizer is then

$$\frac{d[M^+]}{dt}\frac{1}{[M]} = I_e \sigma = 6 \times 10^{16} \times 10^{-16} = 6 \qquad (56.14)$$

However, product molecules arriving in the detector are not stationary. Typically product velocities are on the order of 500m/s. If the ionization region has a length of 1 cm, the residence time of a product molecule is on the order of 2×10^{-5} s. Consequently, the ionization probability of product molecules passing through the ionizer is

$$\frac{d[M^+]}{dt}\frac{1}{[M]} = 2 \times 10^{-5} \times 6 = 1.2 \times 10^{-4} \qquad (56.15)$$

Although this does not appear very efficient (indeed, it is 4 orders of magnitude less so than surface ionization), nevetheless if the background count rate is sufficiently low then good statistics may be obtained with signal levels as low as 1 Hz. Thus, for electron impact ionization based detection, a key factor determining the sensitivity of the experiment is the background count rate at the masses of interest.

Spectroscopic Detection

Spectroscopic detection methods usually involve either laser- induced fluorescence (LIF) or resonant photoionization (REMPI) ??. Alternative techniques such as laser-induced grating methods and non-resonant VUV photoionization are also being applied to scattering experiments. Essential to the use of spectroscopic methods for reactive scattering studies is an understanding of the spectrum of the species of interest. This may be challenging for many reactive systems because the products may be produced in highly excited vibrational or electronic states that may not be well characterized. Additional spectroscopic data may be required depending on the nature of the experiment. Franck-Condon factors are necessary to compare the intensities of different product vibrational states, while a calibration of the relative intensities of different electronic bands requires a measure of the electronic transition moments. In some cases one must include the specific dependence of the electronic transition moment on the internuclear distance by integrating over the vibrational wave function. Populations corresponding to different rotational lines may be compared after the appropriate correction, which is represented by the Hönl-London factors only for isotropic irradiation and detection. This is certainly not the case for most laser-based experiments. Generally, the detailed dependence of the excitation and detection on the relevant magnetic sublevels must be considered[26, 27, 28]. Caution is required in using any spectroscopic method involving at some stage a level that is predissociated. This may lead to a dramatic decrease in the associated fluorescence or photoionization yield if the predissociation rate approaches or exceeds the rate of fluorescence or subsequent photionization.

An important question in any experiment based on spectroscopic detection is whether product flux or number density is probed. This question is considered in detail in several articles[12, 29]. It depends on the lifetime of the state that is probed, the relative time that the molecule is exposed to the probe laser field, and its residence time in the interaction region. Saturation phenomena are also important, yet not necessarily easily anticipated. Complete saturation does not readily occur because excitation in the wings of the laser beam profile becomes more significant as the region in the center of the beam becomes saturated [30].

Laser-induced fluorescence (LIF) is currently the most widely used spectroscopic technique employed in inelastic and reactive scattering experiments[25, 26, 32]. It has been used to measure state- resolved total cross-sections[31] and differential cross sections in electronic[33], vibrational and rotationally inelastic scattering[11] as well as reactive scattering[34].

With the development of high-power tunable lasers and the discovery of useful photoionization schemes, res-

onant multi-photon ionization (REMPI) is becoming a more general technique[35, 36]. REMPI has the advantages associated with ion detection, namely considerable convenience in mass selection and efficient detection, in addition to the capability for quantum state selectivity. Disadvantages associated with REMPI arise primarily as a result of the higher laser power employed in these detection schemes compared with LIF. Caution is required in attempting to extract quantitative information from resonant photoionization spectra because one is often compelled to work in regimes in which one or several of the steps involved in the ionization process are saturated. This is of particular concern at the high laser powers necessary for multiple photon transitions. A related alternative to direct photoionization involves excitation of products to metastable Rydberg states followed by field ionization some distance from the interaction region. This technique has the advantage of very low background and is capable of extraordinary time-of-flight resolution. Remarkable results have recently been obtained for the reaction D+H_2 using this method[37]. Photoionization techniques are becoming more widely used in scattering experiments as the basis for product imaging detection schemes discussed below.

56.2.4 A Typical Signal Calculation

We now present a typical signal calculation for a crossed beam scattering experiment. For an experimental system in which a beam of atoms A collides with a beam of molecules B yielding products C and D, the rate of formation of C is given by

$$\frac{dN_C}{dt} = n_A n_B \sigma_r g \Delta V \qquad (56.16)$$

where n_A and n_B are the number densities of the respective reagents at the interaction region, σ_r is the reaction cross section, g the magnitude of the relative velocity between the reactants and ΔV the volume of intersection of the beams. For a typical experiment employing continuous supersonic beams, the number densities of the atomic and molecular reactants are on the order of 10^{11} and $10^{12}/\text{cm}^3$ and the scattering volume 10^{-2}cm^2. For a relative velocity of 10^5 cm/s and reaction cross section of 10^{-15} cm^2, the rate of product formation $dN_c/dt = 10^{11}$ molecules/s. The kinematics and energetics of the reaction will then determine the range of laboratory angles into which the products will scatter, and the magnitude of the scattered signal.

If the products scatter into 1 sr of solid angle in the laboratory and the detector aperture is 3×10^{-3} sr (roughly 1 degree in both directions perpendicular to the detector axis), then the detector will receive 3×10^7 product molecules/s. Given the detection probability obtained above, we will detect 3600 product ions/s. This is adequate to obtain very good statistics in a short time as long as the background count rate is not considerably higher than this number.

For a nonspecific detection technique such as electron bombardment ionization coupled with mass filtering, it is necessary to use ultrahigh vacuum (10^{-10} torr) in the detector region to minimize interference from background gases. Under these conditions the residual gases are primarily H_2 and CO, with number densities on the order of 10^6 cm^3. Differential pumping stages, each of which may reduce the background by 2 orders of magnitude, are generally used to lower the background from gases whose partial pressures are lower than the ultrahigh vacuum limit of the detector chamber. However, this differential pumping will help only for those molecules that do not follow a straight trajectory through the detector. The contribution from the latter is given by

$$n' = \frac{nA}{4\pi x^2} \qquad (56.17)$$

where n is the number density of molecules effusing from an orifice of area A and n' is their number density at a distance x on axis downstream. For a distance of 30 cm and a main chamber pressure of 3×10^{-7} torr, this corresponds to a steady state density of 10^5 molecules/cm^3 at the ionizer, a reduction of 6 orders of magnitude. Three stages of differential pumping are thus the maximum useful under these conditions, since the primary source of background will then be molecules following a straight trajectory from the main chamber. It may then be useful to employ a liquid helium cooled surface opposite the detector entrance to minimize scattering of background molecules into the ionizer.

56.3 EXPERIMENTAL CONFIGURATIONS

56.3.1 Crossed-beam Rotatable Detector

This configuration, schematically illustrated in Fig. 56.1 represents a standard now used at many laboratories throughout the world[38]. It is most commonly employed as illustrated, with two continuous beams fixed at 90 degrees. The molecular beam sources are differentially pumped and collimated to yield an angular divergence of about 2 degrees. The beams cross as close as possible to the nozzles, with a typical interaction volume of $(3mm)^3$. Scattered products pass through an aperture on the front of the detector, thence through several stages of differential pumping, before reaching the ionizer. Ions formed by electron impact on the neutral products are then extracted into a quadrupole mass spectrometer with associated ion counter. A chopper wheel is generally used at the entrance to the detector to provide a time origin for

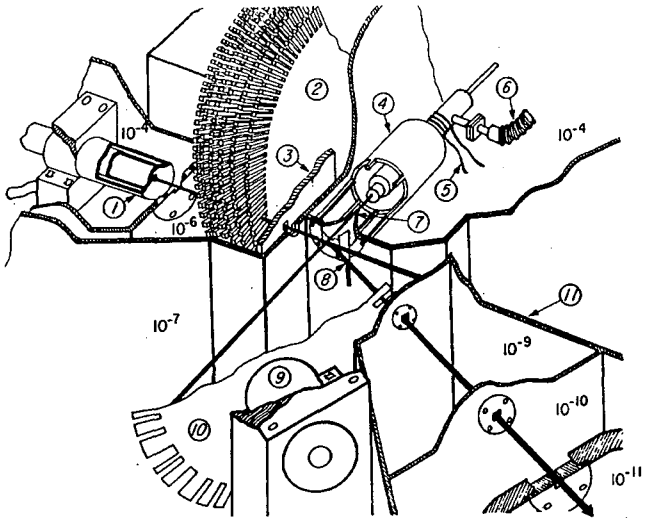

Figure 56.1. Schematic view of crossed molecular beam apparatus with rotatable quadrupole mass spectrometer detector.

recording time-of-flight spectra. Pseudorandom sequence chopper disks provide optimal counting statistics while maintaining a high duty cycle (50%)[39]. The detector may be rotated about the interaction region, typically through a range of 120 degrees or so, allowing one to examine products scattered at a range of laboratory angles. In addition to time-of-flight detection, one of the beams may be gated on and off for background subtraction and the detector moved to record integrated signal at each laboratory angle.

Two kinds of measurements are typically made in these experiments: time-of-flight spectra and angular distributions. Usually one is interested in obtaining the complete product flux- velocity contour map, since this contains the full details of scattering process. This is obtained by measuring a full angular distribution as well as time-of-flight data at many laboratory angles. The results are then simulated using a "forward convolution" fitting procedure to obtain the underlying contour map[40, 77, 42]. Because scattering of isotropic reagents exhibits cylindrical symmetry about the relative velocity vector, it is sufficient to measure products scattered in any plane containing this vector to determine the product distribution. This is not true for structured particles (involving atoms in P states, for example ??); this azimuthal anisotropy has been used to explore the impact parameter dependence of the reaction dynamics[43]. In a typical reactive scattering experiment, $A+BC \rightarrow AB+C$, either of the two products may be detected. Conservation of linear momentum requires that the center-of-mass frame momenta of the two products must sum to zero. It is thus only necessary to obtain the contour map for one of the products. The choice of detected product is usually dictated by kinematic considerations, although one may choose to detect a product that is kinematically disfavored if its partner happens to possess a high-background mass. Kinematic considerations can be critical in assessing the suitability of a given system for study. It is very important that one of the products be scattered entirely in the viewing range of the detector in order to obtain a complete picture of the reaction dynamics.

The advantages of crossed-beams employed in conjunction with an electron impact ionizer-mass spectrometer detector derive primarily from the universality of the detector. No spectroscopic information is required and there are no dark channels. In addition, the resolution of these machines may be increased almost arbitrarily; indeed, even rotationally inelastic scattering has been studied using this approach[44]. The disadvantages in general are complementary to the advantages: the universal detector implies that quantum state resolution is not achieved directly, although in favorable cases the product vibrational states may be resolved in the translational energy distributions [19, 45]. In addition, if the product of interest represents a mass that receives interference from one of the beam masses, background interference may be problematic. Kinematic considerations mentioned above may also preclude study of certain systems. However, the kinematic requirements for the Doppler and imaging approach are discussed below are complementary to those of the rotatable-detector configuration.

56.3.2 Doppler Techniques

Much effort has been exerted toward developing spectroscopic detection methods in crossed-beam experiments, since the measurement of state-resolved differential cross sections represents the ultimate level of insight into the reaction dynamics. In the late 70's Kinsey proposed using product Doppler profiles to obtain differential cross sections using LIF[46]. By the early 80's, Kinsey and others reported measurements of prod-

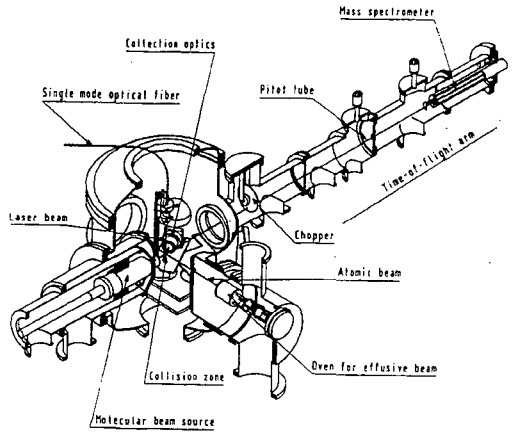

Figure 56.2. Schematic view of crossed molecular beam apparatus with LIF-Doppler detection.

uct Doppler profiles recorded with a laser directed parallel to the relative velocity vector, dubbed ADDS (Angular Distributions by Doppler Spectroscopy)[47]. Owing to the Doppler shift, a particle scattered with a center of mass velocity of $\overrightarrow{u}$ will perceive the photon as having a frequency

$$\nu' = \nu\left(1 - \frac{(\overrightarrow{u} + \overrightarrow{V_{cm}}).\hat{\mathbf{n}}}{c}\right) \qquad (56.18)$$

where ν is the laser frequency in the laboratory, $\overrightarrow{V_{cm}}$ is the velocity of the center of mass in the laboratory and $\hat{\mathbf{n}}$ is the unit vector in the probe laser direction. Kinsey showed that, for the case of a single possible recoil speed, one may obtain the full differential cross section directly in the center- of-mass frame by reconstruction of a single Doppler profile. In this case the angular resolution is a maximum for the sideways scattered products, and a minimum at the poles. An alternative approach is to measure the Doppler profile with a laser perpendicular to the relative velocity vector. This approach ("PADDS" for Perpendicular ADDS) affords complementary angular resolution but folds the forward and backward scattered products into a single symmetric component[?]. For the case in which the detected product does not possess a known recoil speed (for example if the thermodynamics of the process are not known, or if one probes the atomic fragment in an $A + BC \rightarrow AB + C$ reaction), a single Doppler profile is insufficient to reconstruct the double differential cross sections. Nevertheless, Kinsey's earliest experimental results were for one such example: the reaction $H + NO_2 \rightarrow OH + NO$. This experiment was somewhat handicapped by poor resolution, however[48].

More recently Mestdagh and coworkers at Saclay have studied electronically inelastic collision processes using this approach by measuring the Doppler profiles over a range of probe laser angles. This technique is schematically illustrated in Fig. 56.2. A beam of barium atoms is crossed at 90 degrees by a beam of some molecular perturber. At the interaction region, the barium atoms are electronically excited using a narrow band dye laser. Scattered barium atoms that have undergone a specific electronic transition as a result of the collision are probed at the interaction region using a second dye laser, which is scanned across the Doppler profile. The product flux-velocity contour map was then reconstructed by means of a forward convolution simulation procedure analogous to that commonly employed in the analysis described in the preceding section.

The advantages of the Doppler methods are primarily a consequence of the fact that they are spectroscopic in nature, so that state-resolved detection is possible. In the experiments at Saclay, for example, near-resonant inelastically scattered barium atoms were detected directly superimposed on the barium beam, despite six orders of magnitude difference in intensity. Another difference between the Doppler methods and the traditional crossed-beam configuration is that the kinematic considerations favor detection of fast particles, and almost any system that is spectroscopically suitable may be considered. The primary disadvantage of Doppler methods is the limited angular and translational energy resolution possible. Often, however, modest angular resolution is all that is necessary to achieve a global picture of the reaction dynamics. Much current work involves application of Doppler methods to study photoinitiated reactions in cells, relying on the short excited state lifetimes to guarantee single collision conditions and using iterative fitting procedures to gain insight into product velocity distributions and angular momentum polarization[49]. As in all scattering experiments relying on spectroscopic detection, the importance of the latter must be investigated experimentally since it can have a profound effect on the measured distributions. Properly understood, product angular momentum polarization can afford a powerful additional means of exploring the collision dynamics. Examples of 3- and 4-vector correlation experiments approach a "complete description" of the scattering process ?? [50, 51, 52].

56.3.3 Product Imaging

Another spectroscopic technique to emerge in recent years is one based on direct imaging of the scattered product distribution. The technique was developed by Chandler and Houston and first used to record state-resolved angular distributions of methyl radicals from the 355 nm photodissociation of methyl iodide[53]. The method has since been widely employed to study photodissociation, and more recently it has been used to record state-resolved inelastic scattering in a crossed-beam experiment[54]. Recently it has been applied for the first time to a crossed- beam reactive scattering system[55]. The crossed-beam configuration used by Houston and coworkers is shown schematically in Fig. 56.3. The two skimmed supersonic beams cross at

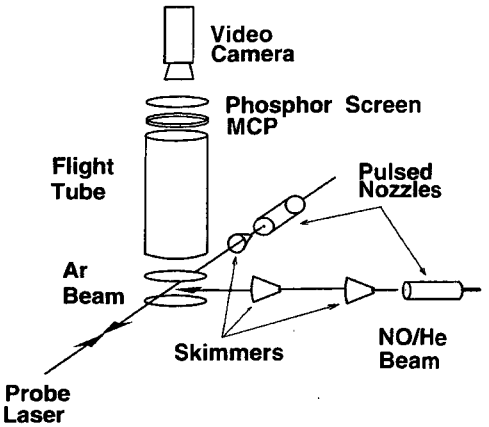

Figure 56.3. Schematic view of crossed molecular beam apparatus with product imaging detection.

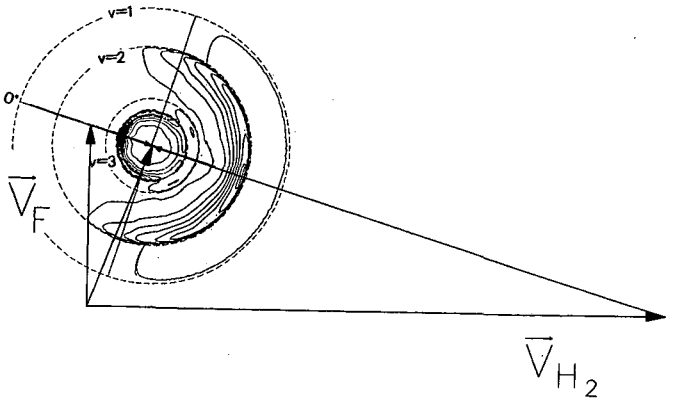

Figure 56.4. Newton diagram for collision of F with D_2 with superimposed center-of-mass flux-velocity contour map.

right angles, and scattered products are state- selectively ionized on the axis of a Wiley- McLaren time-of-flight mass spectrometer using resonant photoionization. The ion cloud thus formed continues to expand with its nascent recoil velocity as it drifts through the flight tube. The ions then strike a microchannel plate coupled to a phosphor screen. The latter is viewed by a video camera gated to record the signal at the mass of interest. The images are thus two-dimensional projections of the nascent three dimensional product distributions.

Some means of regenerating the three dimensional distribution from the projection must be employed, and there exist two alternatives currently in use. The first, a tomographic reconstruction using an inverse Abel transform, is widely used in photodissciation studies[56, 57]. It is a direct inversion procedure feasible for cases in which the image is the projection of a cylindrically symmetric object, with its axis of symmetry parallel to the image plane. This analysis yields a unique product contour map directly from the image, but it is difficult to incorporate apparatus functions, and is sensitive to noise in the data. Alternatively, a forward convolution fitting method may be used as above. A Monte Carlo based simulation was used to obtain the differential cross sections for the Ar-NO results, and this method has the advantage that one may treat the averaging over experimental parameters quite rigorously.

The advantages of the imaging method again derive from the fact that it relies on a spectroscopic probe, so that quantum state resolution is possible and background interference may be avoided. In addition it possesses a multiplexing advantage since the velocity distribution is recorded for all angles simultaneously. Imaging relies exclusively on photoionization, unlike the Doppler methods which may employ either photoionization or laser-induced fluorescence. This is somewhat disadvantageous since the available photoionization schemes are limited and often high laser power is necessary to achieve adequate signal intensity. As a result, background ions can be a problem. In general 1+1 detection schemes are thus preferable.

56.3.4 Laboratory to Center-of-Mass Transformation

In a crossed molecular beam experiment, the angular and velocity distributions measured in the laboratory do not allow for direct interpretation of the scattering process. One must transform the measured distributions from the laboratory frame to the center-of-mass coordinate system. Accounts of this transformation and details concerning the material presented below may be found in references [58, 59, 60, 61], among others. The Newton diagram is useful to aid in visualizing the transformation, and in understanding the kinematics of a given collision system. For the scattering of F+D_2 for example, shown in Fig. 56.4, a beam of fluorine atoms with a velocity $\mathbf{v}_F$ is crossed by a beam of D_2, velocity $\mathbf{v}_{D_2}$, at 90 degrees. The relative velocity between the two reactants g, is given by $\mathbf{v}_F - \mathbf{v}_{D_2}$, and the velocity vector of the center-of-mass of the entire system is given by

$$\mathbf{V}_{cm} = \frac{M_F \mathbf{v}_F + M_{D2} \mathbf{v}_{D_2}}{M_F + M_{D_2}} \qquad (56.19)$$

The center-of-mass velocity vector divides the relative velocity vector into two segments corresponding to the center-of-mass velocities of the two reagents. The magnitude of these vectors, u_F and u_{D_2} are inversely proportional to the respective masses. If scattered DF products are formed with a laboratory scattering angle Θ and a laboratory velocity $\mathbf{v}_{DF}$ as shown in Fig. 56.4, this corresponds to DF *backscatterred* with respect to the incident F atom, in the center-of-mass system. It is common to refer the scattering direction to the atomic reagent in an $A + BC \rightarrow AB + C$ reaction, for example, to make clear the dynamics of the process. In this case the backscattered DF arises as a result of a direct rebound collision.

Some useful kinematic quantities are summarized here. For beams A and BC intersecting at 90 degrees the angle of the center-of-mass velocity vector with respect to A is given by:

$$\Theta_{cm} = \arctan \frac{M_{BC} v_{BC}}{M_A v_A} \tag{56.20}$$

For an arbitrary Newton diagram with angle α between the two beams the magnitude of the relative velocity is given by:

$$g^2 = v_A^2 + v_{BC}^2 - 2 v_A v_{BC} \cos\alpha \tag{56.21}$$

the relative velocity vector is given by

$$\mathbf{g} = \mathbf{v}_A - \mathbf{v}_{BC} \tag{56.22}$$

and the collision energy is

$$E_{coll} = \frac{1}{2}\mu_i g^2. \tag{56.23}$$

where μ_i is the reduced mass of the initial collision system. The magnitude of the center of mass frame velocity of particle A before collision is

$$\mathbf{u}_A = \frac{m_{BC}}{m_A + m_{BC}}\mathbf{g} \tag{56.24}$$

The final relative velocity is

$$\mathbf{g}' = \mathbf{v}_{AB} - \mathbf{v}_C \tag{56.25}$$

with its magnitude given by

$$g' = \sqrt{\frac{2E_{avail}}{\mu_f}} \tag{56.26}$$

where the available energy E_{avail} is given by

$$E_{avail} = E_{coll} + E_{int,reac} + E_{exo} - E_{int,prod} \tag{56.27}$$

in which $E_{int,reac}$ is the internal energy of the reactants, E_{exo} is the exoergicity of the reaction and $E_{int,prod}$ is the internal energy of the products.

One must transform the recorded laboratory signal intensity $I(\Omega)(\equiv \frac{d^2\sigma}{d^2\Omega})$ into $I(\omega)(\equiv \frac{d^2\sigma}{d^2\omega})$, the corresponding center-of-mass quantity. For the traditional crossed-beam configuration described in 56.3.1, the laboratory distributions are distorted by a transformation Jacobian that arises because the laboratory detector views different center-of-mass frame solid angles depending on the scattering angle and recoil velocity. For the spectroscopic experiments described in 56.3.2 and 56.3.3, the laboratory to center-of-mass tranformation Jacobian is unity (the center of mass velocity represents a simple frequency offset of the Doppler profiles, for example); however, the transformation of the scattering distributions from the recorded quantities (2-dimensional projections or intensity vs. wavelength) to recoil velocity distributions may be complex. Two cases must be considered for the configuration discussed in 56.3.1: one in which discrete velocities result (such as elastic or state-resolved scattering experiments) and one in in which continuous final velocities are measured. For the first case, the laboratory and center-of-mass differential cross sections are independent of the respective product velocities v and u and these quantities are related by:

$$\frac{d^2\sigma}{d^2\Omega} = J\frac{d^2\sigma}{d^2\omega} \tag{56.28}$$

so that the transformation Jacobian is given by

$$J = \frac{d^2\omega}{d^2\Omega} \tag{56.29}$$

For discrete recoil velocities note that the center-of-mass solid angle is

$$d^2\omega = \frac{dA}{u^2} \tag{56.30}$$

where dA is a surface element of the product Newton sphere. The laboratory solid angle corresponding to this quantity is

$$d^2\Omega = \frac{\cos(\mathbf{u},\mathbf{v})}{v^2} dA \tag{56.31}$$

so that the Jacobian for the first case is given by

$$J = \frac{v^2}{u^2 \cos(\mathbf{u},\mathbf{v})} \tag{56.32}$$

For the case of continuous final velocities, the differential cross sections are velocity-dependent and are related as

$$\frac{d^3\sigma}{d^2\Omega\, dv} = J\frac{d^3\sigma}{d^2\omega\, du} \tag{56.33}$$

so that here the Jacobian is given by

$$J = \frac{d^2\omega\, du}{d^2\Omega\, dv} \tag{56.34}$$

In this case we consider a recoil volume element $d\tau$ (in velocity space), which must be the same in both coordinate frames:

$$d\tau_{cm} = u^2\, du\, d^2\omega = d\tau_{lab} = v^2\, dv\, d^2\Omega \tag{56.35}$$

so that the Jacobian is

$$J = \frac{v^2}{u^2}. \tag{56.36}$$

In this case then, the laboratory signal intensity is related to that in the center-of-mass by

$$I_{lab}(\Theta, v) = \frac{v^2}{u^2} I_{cm}(\theta, u). \tag{56.37}$$

For a mass spectrometer detector with electron bombardment ionizer one measures number density of particles rather than flux, so that the recorded signal is given by

$$N_{lab}(\Theta, v) = \frac{I_{lab}(\Theta, v)}{v} = \frac{v}{u^2} I_{cm}(\theta, u). \qquad (56.38)$$

The usual flux-velocity contour map is a polar plot of the quantity $I_{cm}(\theta, u)$. The product velocity distributions then are given by

$$I(u) = \int\int I(\theta, u) \sin\theta d\theta d\phi = 2\pi \int_0^\pi I(\theta, u) \sin\theta d\theta \qquad (56.39)$$

and the translational energy distributions by

$$I(E_T) = I(u) \left| \frac{du}{dE_T} \right|. \qquad (56.40)$$

56.4 ELASTIC AND INELASTIC SCATTERING

56.4.1 Introduction

When particles collide they may exchange energy or recouple it into different modes, they may change their direction of motion, and they may even change their identity. The study of these processes reveals a great deal of information about the forces acting between the particles and their internal structure. It is useful to begin a consideration of the kinds of chemical information one may derive from reactive scattering studies first with a summary of the dominant features of elastic and inelastic scattering.

56.4.2 The Differential Cross Section

Fig. 56.5 illustrates the relation between the deflection function χ and the impact parameter b for a realistic potential containing an attractive well and a repulsive core. For large impact parameters there is no interaction, hence no deflection. At smaller values of b, the attractive part of the potential is experienced and some positive deflection results. At a smaller value of b, b_r, the influence of the attractive component of the potential reaches a maximum, giving the greatest positive deflection: this is the rainbow angle by analogy with the optical phenomenon. There is another value of the impact parameter at which point the attractive and repulsive parts of the potential will balance yielding no net deflection. This is the 'glory impact parameter' b_g. For yet smaller values of b, the interaction is dominated by the repulsive core and rebound scattering gives a negative deflection function.

The important expressions related to the differential cross section are summarized here[62]. For scattering

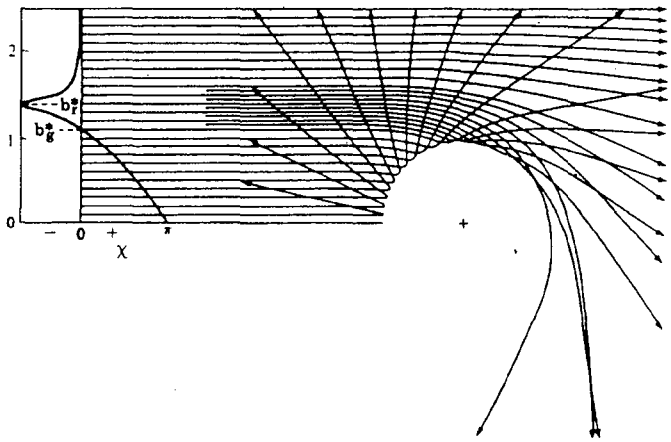

Figure 56.5. Schematic diagram showing relation between impact parameter b and deflection function .

involving an isotropic potential, the deflection angle $\Theta = |\chi|$. The differential cross section gives the rate of all collisions leading to deflection angles in the solid angle element $d\omega$:

$$\frac{dN(\theta)}{dt} \propto I(\theta)d\omega = I(\theta)2\pi \sin(\theta)d\theta \qquad (56.41)$$

The incremental cross section is $d\sigma = I(\theta)d\omega = 2\pi b db$, so

$$I(\theta) = \frac{b}{\sin\theta(\frac{d\theta}{db})}. \qquad (56.42)$$

For classical particles, the relation between the deflection function and the potential is

$$\chi = \pi - 2b \int_{R_0}^{\infty} \frac{dR}{R^2} (1 - \frac{V(R)}{E_T} - \frac{b^2}{R^2})^{-1/2} \qquad (56.43)$$

where $V(R)$ is the potential as a function of interparticle distance R, R_0 is the turning point of the collision and E_T the collision energy.

In the high energy limit, for large impact parameters ($R_0 \approx b$)

$$\chi(b, E_T) \propto \frac{V(b)}{E_T} \qquad (56.44)$$

For a long-range potential $V(R)$ proportional to R^{-s},

$$E_T^{2/s} \theta^{2(1+1/s)} I(\theta) = \text{const.} \qquad (56.45)$$

For a potential exhibiting a minimum, the rainbow angle θ_r is proportional to the collision energy, and clearly resolved when the collision energy is 3 to 5 times the well depth. In addition, supernumery rainbows and quantum mechanical "fast osillations" occur in the differential cross section, and these provide a sensitive probe of the interaction. Highly accurate interatomic potentials are routinely obtained from elastic scattering experiments[60, 65].

56.4.3 Rotationally Inelastic Scattering

Classical scattering involving an anisotropic potential results in another rainbow phenomenon, distinct from that seen in pure elastic scattering and notable in that it does not require an attractive component in the potential. These rotational rainbows are equivalently seen in a plot of integral cross section against change in rotational angular momentum Δj, or in the differential cross section for a particular value of Δj. The rotational rainbow peaks are a consequence of the fact that many orientation angles γ are possible in a collision involving an anisotropic potential, and when there is a minimum in $d\gamma/d\theta$ for a given Δj, the differential cross section reaches a maximum[63]. The rotational rainbow peak occurs at the most forward classsically allowed value of the scattering angle and the differential cross section drops rapidly at smaller angles. The rainbow moves to more backward angles with increasing Δj because the larger j-changing collisions require greater momentum transfer, hence must arise from lower impact parameter collisions. For heteronuclear molecules two rainbow peaks may be observed, corresponding to scattering off of either side of the molecule. One can relate the location of the rainbow peak to the shape of the potential using a classical hard ellipsoid model[64]:

$$A - B = \frac{j}{p_0}\left(2\sin\left(\frac{\theta_{r,cl}}{2}\right)\right)^{-1} \qquad (56.46)$$

where j is the rotational angular momentum, p_0 is the inital linear momentum, $\theta_{r,cl}$ is the "classical" rainbow position, and A and B are the semi-major and semi-minor axes of a hard ellipse potential. The classical rainbow positions are found to occur somewhat behind the quantum mechanical and experimental rainbow positions, so the classical rainbow may be estimated as the point at which the peak has fallen to 44% of the experimental value. Real molecular potentials may be far from ellipsoids, however, so detailed quantitative insight into the potential requires a comparison of scattering data with trajectory calculations.

56.4.4 Vibrationally Inelastic Scattering

There has been no direct observation of the differential cross section of T-V or V-T energy transfer involving neutral molecules owing to the small cross sections for these processes. Integral cross section data is available, however. Above threshold, the latter has shown a linear dependence of cross section on collision energy for $\Delta\nu = 1$, quadratic for $\Delta\nu = 2$ and cubic for $\Delta\nu = 3$[66]. In addition, a great deal of information on vibrational relaxation processes has been obtained in cell experiments[67].

56.4.5 Electronically Inelastic Scattering

A wealth of information is available on electronically inelastic scattering systems, since these in general exhibit much larger cross sections than V-T processes[68, 69]. In addition, spectroscopic methods may be used to overcome some of the background problems that hamper the study of the latter. Often quenching of electronically excited states involves curve crossing mechanisms, so that very effective coupling of electronic to vibrational energy may occur. Spin-orbit changing collisions of $Ba(^1P)$ with O_2 or NO, for example, occur by a near-resonant process and result in almost complete conversion of electronic energy to vibrational excitation of the product[70]. The analogous collisions with N_2 and H_2, however, reveal very repulsive energy release with little concomitant vibrational excitation. Both processes likely occur via curve crossings of the relevant electronic states, but the near-resonant mechanism occurs by way of an ionic intermediate.

56.5 REACTIVE SCATTERING

56.5.1 Introduction

The dynamics of reactive collisions fall broadly into three main categories characterized by distinct angular and energy distributions. These distributions can be used to determine thermodynamic quantities for unstable radical products, to identify product channels and reaction mechanisms, and to infer information about the shape of the potential energy surface or surfaces involved in the reaction. The three categories are 1)Harpoon/stripping reactions, 2) Rebound reactions and 3) Long-lived complex formation. Some reactions may exhibit more than one of these mechanisms at once, or the dynamics may change from one to another as the collision energy is varied.

56.5.2 Harpoon/stripping reactions

It was known in the 1930's that collisions of alkali atoms with halogen molecules exhibit very large cross sections and yield highly excited alkali halide products. These observations were accounted for by the "harpoon" mechanism proposed by M. Polanyi: because alkali atoms have low ionization potentials and halogen molecules large electron affinities, as the alkali atom approaches the molecule electron transfer may occur at long range. These processes are considered in detail in chapter ??. [71, 72] The "harpooning" distance R_c at which this curve crossing takes place may be estimated simply as the distance at which the Coulomb attraction of the ion

pair is sufficient to compensate for the endoergicity of the electron transfer:

$$R_c = \frac{2}{E_{IP} - E_{EA}} \qquad (56.47)$$

where E_{IP} and E_{EA} represent the ionization potential and electron affinity of the electron donor and recipient, respectively. For R in angstroms and E in eV, this relation is

$$R_c = \frac{14.4}{E_{IP} - E_{EA}} \qquad (56.48)$$

Owing to the large Coulombic attraction between the ion pair, reaction proceeds immediately following electron transfer. The crossing distance may then be used to estimate the effective reaction cross section. The vertical electron affinity is not necessarily the appropriate value to use in estimating these crossing distances; stretching of the halogen bond may occur during approach, so the effective electron affinity is generally somewhere between the vertical and adiabatic values. Often there exists some repulsion between the atoms in the resulting halogen molecular ion, so that electron transfer is accompanied by dissociation of the molecule in the strong field of the ion pair. The alkali ion, having sent out the electron as the "harpoon", then reels in the negative ion leaving the neutral halogen atom nearly undisturbed as a spectator. Because these events occur at long range, there is no momentum transfer to the spectator atom and it is a simple matter to estimate the anticipated angular and translational energy distributions in this "spectator stripping" limit. The scattered product molecule is directly forward scattered (referred to the direction of the incident atom) and for the reaction $A + BC \rightarrow AB + C$, the final center of mass velocity for the product AB is given by:

$$\mathbf{u}'_{AB} = -\frac{M_C \mathbf{u}_{BC}}{M_{AB}} \qquad (56.49)$$

where $\mathbf{u}_{BC}$ is the initial center-of-mass velocity of the BC molecule. This spectator stripping mechanism may occur in systems other than harpoon reactions, and is useful to remember as a limiting case.

The likelihood of electron transfer at these crossings may be estimated using a simple Landau-Zener model[72]. For relative velocity g, impact parameter b and crossing distance R_c, the probability for undergoing a transition from one adiabatic curve to another (that is, the probability for remaining on the diabatic curve) is given by

$$p = 1 - e^{-\delta} \qquad (56.50)$$

where

$$\delta = \frac{2\pi H_{12}^2 R_c^2}{g}\left(1 - \frac{b^2}{R_c^2}\right)^{-\frac{1}{2}} \qquad (56.51)$$

and H_{12} is the coupling matrix element between the two curves. The coupling matrix element may be estimated from an empirical relation which is accurate within a factor of three over a range of 10 orders of magnitude for the coupling matrix element[73]. In atomic units:

$$H_{12} = \sqrt{I_1 I_2} R_c^* e^{(-0.86 R_c^*)} \qquad (56.52)$$

where

$$R_c^* = (\sqrt{I_1} + \sqrt{I_2}) \qquad (56.53)$$

is the reduced crossing distance and I_1 and I_2 are the initial and final ionization potentials of the transferred electron (again, in atomic units). One finds electron transfer probabilities near unity for curve crossing distances below about 5 angstroms, dropping to zero for crossing at distances greater than about 8 angstroms. These estimates are based on electron transfer in atom-atom collisions, and it is important to remember that atom-molecule collisions occur on surfaces rather than curves, so the crossing seam may cover a broad range of internuclear distances.

56.5.3 Rebound reactions

Another common direct reaction mechanism is the "rebound" reaction exemplified by $F+D_2 \rightarrow DF + D$[19]. The center-of-mass product flux-velocity contour map obtained for this reaction is shown in Fig 56.4. Owing to the favorable kinematics and energetics in this case, the FD product vibrational distribution is clearly resolved, and seen to peak at v=2. The dominant v=2 product peaks at a center of mass angle of 180 degrees (referred to the direction of the incident F atom.) This rebound scattering is characteristic of reactions exhibiting a barrier in the entrance channel. Rebound scattering implies low impact parameter collisions, and this serves to couple the translational energy efficiently into overcoming the barrier. Low impact parameter collisions are necessarily smaller cross section events however, since cross section scales quadratically with the impact parameter.

56.5.4 Long-lived complexes

A third important reaction mechanism involves the formation of an intermediate that persists for some time before dissociating to give products. If the collision complex survives for many rotational periods (10^{-11} s, certainly a long time on a molecular scale), then the center-of- mass angular distribution will exhibit a characteristic forward- backward symmetry, usually with peaking along the poles. The latter occurs because the initial and final orbital angular momenta tend to be parallel (and perpendicular to the initial relative velocity vector.) When there exist dynamical constraints enforcing some other relation, as in the case $F+C_2H_4$, then sideways scattering may be observed despite a lifetime of several rotational periods[74, 75, 76]. For

some systems exhibiting this long-lived behavior, the rotational period may be used as a "molecular clock" to monitor the lifetime of the complex. By increasing the collision energy until the distribution begins to lose its forward-backward symmetry, one can investigate the internal energy of the system just when its lifetime is on the order of a rotational period.

Systems that have an inherent symmetry may exhibit this forward- backward symmetry in the scattering distributions despite lifetimes that are considerably shorter than a rotational period. This is the case for $O(^1D)$ reacting with H_2, for example[77]. This reaction involves insertion of the O atom into the H2 bond resulting in an intermediate that accesses the deep H_2O well and contains considerable vibrational excitation. Trajectory calculations show that the complex dissociates after a few vibrational periods, but the distribution exhibits forward-backward symmetry because the O atom is equally likely to depart with either H atom.

REFERENCES

1. Y. T. Lee, Science, **236**, 793 (1987).
2. W. R. Gentry, *Atomic and Molecular Beam Methods*, Edited by G. Scoles, (Oxford University Press, New York, 1988) ch. , pp. 4 ff.
3. J. B. Anderson, R. P. Andres, and J. B. Fenn, in *Adv. Chem. Phys.* **10**, 275 (1966).
4. D. R. Miller, in *Atomic and Molecular Beam Methods*, Edited by G. Scoles, (Oxford University Press, New York, 1988) ch. , pp. 4 ff.
5. R. Campargue, J. Phys. Chem., **88**, 275 (1984).
6. H. F. Davis, B. Kim, H. S. Johnston and Y. T. Lee, J. Phys. Chem. **97**, 2172 (1993).
7. P. Chen, in *Curr. Top. Ion Phys. Chem.*, C. Y. Ng, ed., in press.
8. R. E. Smalley, Laser Chem., **2**, 167 (1983).
9. M. D. Morse, J. B. Hopkins, P. R. R. Langridge-Smith and R. E. Smalley, J. Chem. Phys. **79**, 5316 (1983).
10. J. G. Pruett and R. N Zare, J. Chem. Phys., **64**, 1774 (1976).
11. K. Bergmann, U. Hefter and J. Witt, J. Chem. Phys., **72**, 4777 (1980).
12. K. Bergmann, in *Atomic and Molecular Beam Methods*, Edited by G. Scoles, (Oxford University Press, New York, 1988) ch. 12.
13. S. J. Sibener, R. J. Buss, P. Cassavechia, T. Hirooka and Y. T. Lee, J. Chem. Phys., **72**, 4341 (1980).
14. R. E. Continetti, B. A. Balko and Y. T. Lee, J. Chem. Phys., **93**, 5719 (1990).
15. P. R. Brooks, Science, **193**, 11 (1976).
16. S. Stolte, Ber. Bunsenges. Phys. Chem. **86** 413 (1982).
17. B. Friedrich and D. R. Herschbach, Nature **353**, 412 (1991).
18. D. Bassi, A. Boschetti, M. Scotoni, and M. Zen, Appl. Phys. B, **26**, 99 (1981).
19. D. M. Neumark, A. M. Wodtke, G. N. Robinson, C. C. Hayden, K. Shobatake, R. K. Sparks, T. P. Schaefer and Y. T. Lee, J. Chem. Phys., **82**, 3067 (1985).
20. M. Faubel, Adv. At. Mol. Phys. **19** 345 (1983).
21. T. R. Touw and J. W. Trischka, J. Appl. Phys. **34**,3635 (1963).
22. Y. T. Lee, J. D. McDonald, P. R. LeBreton and D. Herschbach, Rev. Sci. Intstrum. **40** 1402 (1969).
23. Y. T. Lee, *Atomic and Molecular Beam Methods*, Edited by G. Scoles, (Oxford University Press, New York, 1988) ch. 2, p. 63.
24. R. E. Center and A. Mandl, J. Chem. Phys., **57**, 4104 (1972).
25. R. N. Zare and P. J. Dagdigian, Science **185**, 739 (1974).
26. C. H. Greene and R. N. Zare, J. Chem. Phys., **78**, 6741 (1983).
27. D. A. Case, G. M. McLelland and D. R. Herschbach, Mol. Phys., **35** 541 (1978).
28. G. Hall and P. Houston, Ann. Rev. Phys. Chem. **40**, 375 (1989).
29. D. M. Sonnenfroh and K. Liu, Chem. Phys. Lett., **176**, 183 (1991).
30. N. Billy, B. Girard, G. Gouédard and J. Vigué, Mol. Phys., **61**, 65 (1987).
31. H. Joswig, P. Andresen and R. Schinke, J. Chem. Phys. **85**, 1904 (1986).
32. R. Altkorn and R. N. Zare, Ann. Rev. Phys. Chem. **35**, 265 (1984).
33. J. M. Mestdagh, J. P. Visticot and A. G. Suits in *The Chemical Dynamics and Kinetics of Small Radicals*, K. Liu and W. Wagner, eds., (World Scientific, 1994).
34. S. D. Jons, J. E. Shirley, M. T. Vonk, C. F. Giese and W. R. Gentry, J. Chem. Phys., **92**, 7831 (1992).
35. D. L. Feldman, R. K. Lengel, and R. N. Zare, Chem. Phys. Lett. **52**, 413 (1977).
36. E. E. Marinero, C. T. Rettner and R. N. Zare, J. Chem. Phys. **80** 4142.
37. L. Schneider, K. Seekamp-Rahn, F. Liedeker, H. Stewe and K. H. Welge, Farad. Discuss. Chem. Soc., **91**, 259 (1991).
38. Y. T. Lee, J. D. McDonald, P. R. LeBreton and D. R. Herschbach, Rev. Sci. Instrum. **40**, 1402 (1969).
39. G. Comsa, R. David and B. J. Schumacher, Rev. Sci. Instrum. **52**, 789 (1981).
40. E. Entemann and D. R. Herschbach, J. Chem. Phys. **55**, 4872 (1971).
41. R. Buss, Ph.D. Thesis, University of California, Berkeley, 1972.
42. R. T Pack, J. Chem. Phys. **81**, 1841 (1984).
43. A. G. Suits, H. Hou, H. F. Davis and Y. T. Lee, J.

Chem. Phys. **95**, 8207 (1991).
44. M. Faubel, K.-H. Kohl, J. P. Toennies, K. T. Tang and Y. Y. Yung, Faraday Discuss. Chem. Soc., **73**, 205 (1982).
45. R. E. Continetti, B. A. Balko and Y. T. Lee, J. Chem. Phys. **93**, 5719 (1990).
46. J. L. Kinsey, J. Chem. Phys. **66**, 2560 (1977).
47. J. A. Serri, J. L. Kinsey and D. E. Pritchard, J. Chem. Phys. **75**, 663 (1981).
48. E. L. Murphy, J. H. Brophy, G. S. Arnol, W. L. Dimpfl and J. L. Kinsey, J. Chem. Phys. **70**, 5910 (1979).
49. M. Brouard, S. Duxon, P. A. Enriquez and J. P. Simons, J. Chem. Soc. Faraday Trans., **89**, 1435 (1991).
50. J. M. Mestdagh, J. P. Visticot, P. Meynadier, O. Sublemontier and A. G. Suits, J. Chem. Soc. Faraday Trans. **89**, 1413 (1993).
51. C. J. Smith, E. M. Spain, M. J. Dalberth, S. R. Leone and J. P. J. Driessen, J. Chem. Soc. Faraday Trans. **89**, 1401 (1993).
52. H. A. J. Meijer, T. J. C. Pelgrim, H. G. M. Heideman, R. Morgenstern and N. Andersen, J. Chem. Phys. **90**, 738 (1989).
53. D. W. Chandler and P. L. Houston, J. Chem. Phys. **87** 1445 (1987).
54. L. S. Bontuyan, A. G. Suits, P. L. Houston and B. J. Whitaker, J. Phys. Chem., **97**, 6342 (1993).
55. T. A. Kitsopoulos, D. P. Baldwin, M. A. Buntine, R. N. Zare and D. W. Chandler, Science **260**, 1605 (1993).
56. R. N. Strickland and D. W. Chandler, Appl. Opt. **30** 1811 (1990).
57. K. R. Castleman, *Digital Image Processing* (Prentice Hall, Englewood Cliffs, N.J., 1979).
58. T. T. Warnock and R. B. Bernstein, J. Chem. Phys. **49**, 1878 (1968).
59. R. K. B. Helbing, J. Chem. Phys. **48**, 472 (1968).
60. J. P. Toennies, *in Physical chemistry, an Advanced Treatise, Vol VIA*, W. Jost, ed., (Academic Press, New York, 1974) ch. 5.
61. M. Faubel and J. P. Toennies, Adv. At. Mol. Phys., **13**, 229 (1978).
62. R. D. Levine and R. B. Bernstein, *Molecular Reaction Dynamics and Chemical Reactivity* (Oxford, New York, 1987) ch. 3.
63. R. Schinke and J. Bowman, in *Molecular Collision Dynamics*, J. Bowman, ed. (Springer-Verlag, Berlin, 1983).
64. S. Bosanac, Phys. Rev. A, **22**, 2617 (1980).
65. J. M. Farrar, T. P. Schafer and Y. T. Lee, in *Transport Phenomena*, J. Kestin, ed., A.I.P. Conference Proceedings, No. 11 (1973).
66. G. Hall, K. Liu, M. J. McAuliffe, C. F. Giese and W. R. Gentry, J. Chem. Phys. **81**, 5577 (1984).
67. X. Yang and A. Wodtke, Int. Rev. in Phys. Chem. **12** 123 (1993).
68. I. V. Hertel, Adv. Chem. Phys. **50**, 475 (1982).
69. W. H. Breckenridge and H. Umemoto, Adv. Chem. Phys. **50** 325 (1982).
70. A. G. Suits, P. de Pujo, O. Sublemontier, J. P. Visticot, J. Berlande J. Cuvellier, T. Gustavsson, J. M. Mestdagh, P. Meynadier and Y. T. Lee, J. Chem. Phys. **97**, 4094 (1992).
71. J. Los and A. W. Kleyn, in *Alkali Halide Vapors*, P. Davidovits and D. L. McFadden, eds. (Academic Press, New York, 1979) ch. 8.
72. E. A. Gislason, in *Alkali Halide Vapors*, P. Davidovits and D. L. McFadden, eds. (Academic Press, New York, 1979) ch. 13.
73. R. E. Olson, F. T. Smith and E. Bauer, Appl. Optics, **10**, 1848 (1971).
74. W. B. Miller, S. A. Safron and D. R. Herschbach, Discuss. Faraday Soc. **44** 108 (1967).
75. W. B. Miller, Ph.D. Thesis, (Harvard University, Cambridge, MA, 1969).
76. J. M. Farrar and Y. T. Lee, J. Chem. Phys. **65**, 1414 (1976).
77. R. J. Buss, P. Casavecchia, T. Hirooka and Y. T. Lee, Chem. Phys. Lett., **82**, 386 (1981).

LAWRENCE BERKELEY LABORATORY
UNIVERSITY OF CALIFORNIA
TECHNICAL INFORMATION DEPARTMENT
BERKELEY, CALIFORNIA 94720